Ceramics International 47 (2021) 3643–3648

Contents lists available at ScienceDirect

Ceramics International

journal homepage: www.elsevier.com/locate/ceramint

The effect of a prefabricated crack on the crack growth in ceramics during quenching

Yuqiao Li [a,c], Boyang Liu [b], Xiaohuan Wang [a,c], Yingfeng Shao [a,c,*], Long Li [a,c], Jiachen Wei [a,c], Fan Song [a,c]

[a] State Key Laboratory of Nonlinear Mechanics, Institute of Mechanics, Chinese Academy of Sciences, Beijing, 100190, China
[b] College of Ocean Science and Engineering, Shanghai Maritime University, Shanghai, 201306, China
[c] School of Engineering Science, University of Chinese Academy of Sciences, Beijing, 100049, China

ARTICLE INFO

Keywords:
Thermal shock
Prefabricated crack
Crack interaction
Numerical simulation
Real-time

ABSTRACT

The influence of a prefabricated crack on thermal-shock cracking during quenching is studied in real-time. The results show that after the thermal-shock crack extends to the prefabricated crack, the secondary crack may appear at the lower end of the prefabricated crack. The total vertical length of the crack and the probability of the secondary crack occurrence will gradually increase with the prefabricated crack angle. Besides, the influence of the prefabricated crack distance from the edge on thermal-shock crack growth is also considered. The simulation results of meso-damage mechanics are consistent with experimental observation. This article quantitatively investigates the effect of the prefabricated crack on the thermal-shock crack propagation in ceramics, expanding the research on the mechanism of thermal-shock failure.

1. Introduction

Ceramic materials are extensively used in high-temperature environments due to a high melting point, excellent physico-chemical stability, and perfect high-temperature corrosion resistance [1,2]. However, ceramics are susceptible to thermal-shock damage due to inherent brittleness [3,4], which limits the application range of ceramic materials [2]. Consequently, it is essential to consider and determine the thermal-shock cracking properties of ceramics for appropriate design and engineering applications, which is also valuable for acquiring new knowledge about brittle materials.

Many theoretical studies on thermal-shock cracking have been performed in the last ten years, including energy minimum [5,6], meso-damage mechanics [7,8], phase-field [9], non-local failure [10], bond-based peridynamic [11], and gradient damage models [12,13]. These works confirmed and complemented the obtained findings, which significantly promoted the research of ceramic thermal-shock cracking. Nevertheless, the existing theories did not prove the entire process of the experiments, but only the ultimate result. To improve the agreement between theoretical calculations and the experimental measurements, we propose a method to assess the entire thermal-shock process [14], which has been successfully proved for the quantitative investigation of the crack propagation [8].

Ceramic materials usually contain a certain number of pores or microcracks remained after preparation processes of sintering, cladding, or spraying. The inherent brittleness of ceramics also makes them susceptible to defects during the specific service. The interaction between cracks and preexisting defects were extensively studied in the last decades [15–19]. Generally, micro-defects can shield the main-crack tip, increasing the ceramic toughness [15]. The corresponding experimental works focused on the crack initiation, propagation, and interaction with the prefabricated defects under tensile, compressive, or biaxial loading [16–18]. However, there is little research on the interaction between thermal-shock cracks and inherent defects, because the real-time observation of thermal-shock cracking is not trivial [14]. In this paper, the interaction between thermal-shock cracks and prefabricated cracks will be investigated in the real-time. We perform the quenching test for ceramics with prefabricated cracks and use the meso-damage mechanics model to simulate the interaction between thermal-shock cracks and prefabricated cracks. At the same time, we reveal the influence of the prefabricated crack angle and distance from the edge on the interaction of the cracks.

* Corresponding author. State Key Laboratory of Nonlinear Mechanics, Institute of Mechanics, Chinese Academy of Sciences, Beijing, 100190, China.
E-mail address: shaoyf@lnm.imech.ac.cn (Y. Shao).

https://doi.org/10.1016/j.ceramint.2020.09.215
Received 29 July 2020; Received in revised form 18 September 2020; Accepted 21 September 2020
Available online 22 September 2020

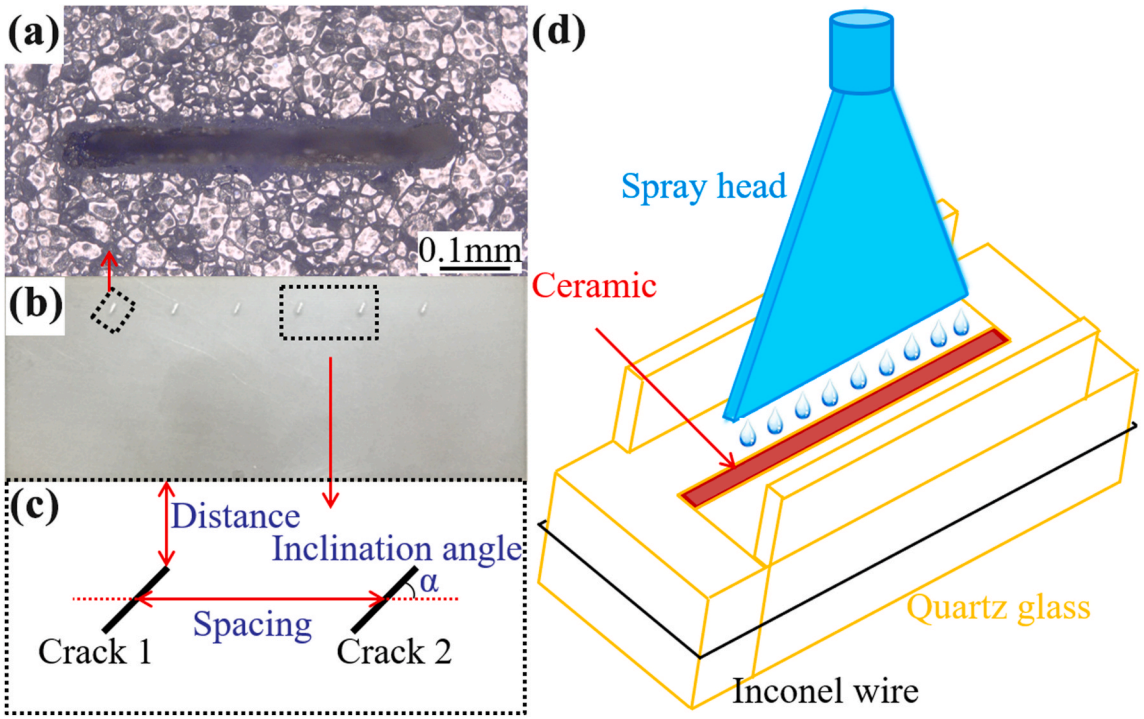

Fig. 1. (a) Prefabricated crack penetrates the specimen thickness on the surface of 20 mm × 50 mm, (b) specimen after laser processing, (c) geometry of two flaws in the thermal-shock specimen, and (d) schematic diagram of the experimental setup.

2. Experiment

2.1. Materials and preparation

Semi-transparent ceramic was made from 0.8 μm Al_2O_3 powder (99.4%, Jiawei Ceramics Co., Ltd., Zhuhai, China) by tape casting and sintering in hydrogen for 2 h at 1700 °C. The average crystalline grain size determined by the average linear intercept method was 20.8 μm, and the density of ceramic measured by the drainage method was 3.95 g/cm^3. A laser (JPT Opto-electronics Co., Ltd., Shenzhen, China) with a power of 20 W and a scan speed of 2 mm/s was used to fabricate a penetrated crack on the surface with a size of 20 mm × 50 mm. The prefabricated cracks with 0.5 mm in length, 0.05 mm in width, a spacing of 3 mm, a distance from the edge of 2 or 4 mm, and an inclination angle of 0, 26.6, 45, or 63.4°, can be successfully introduced in the test specimens by position adjustment, as shown in Fig. 1a–c. The introduction of multiple prefabricated cracks provides a higher probability of interaction with the subsequent thermal shock cracks.

2.2. Quenching test

To generate penetrated cracks, we used a ceramic sheet of 0.5 mm × 20 mm × 50 mm to study the crack morphology under the quenching test. The sheet was placed in a quartz glass clamp with a flume, and then heated to 300 °C and kept 30 min in a muffle furnace. Afterward, it was taken out and placed in a prefocused location within 5 s; then, a nozzle upon the clamp sprayed deionized water at a rate of 5 mL/s at 20 °C. Water flew out by the flume, so the upper surface (0.5 mm × 50 mm) of the sheet suffered from the thermal shock, Fig. 1d. To make the quenching more uniform, we designed the size of the nozzle to be as long as the sheet. Pictures were taken with a Fastcam SA-X2 high-speed camera under quenching at a rate of 10,000 frames/s with a 1024 × 512 pixels resolution, and the crack speed was calculated according to the crack length vs. time.

3. Finite element model of thermal-shock cracking

3.1. Thermo-mechanical calculations

We use ANSYS software to calculate thermo-mechanical fields of the

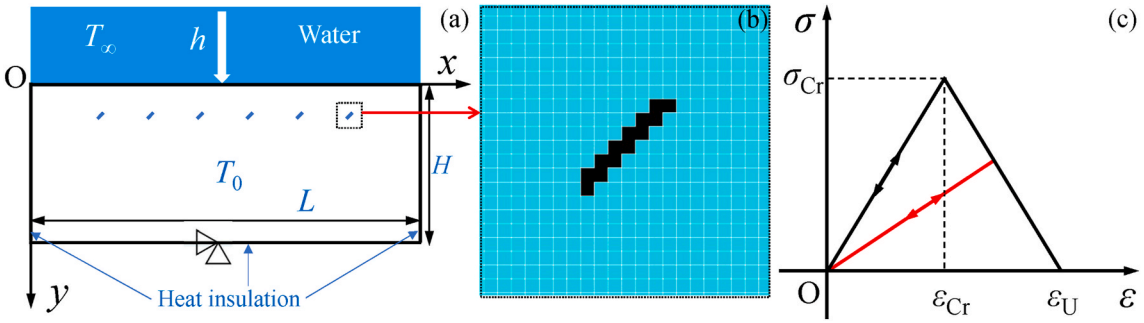

Fig. 2. (a) The finite element model for calculating thermal stress and strain fields, (b) a representative mesh of finite element model including crack, and (c) damage evolution of the mesoscopic element.

Table 1
Mechanical and thermal parameters of alumina used in calculation.

Young modulus E (GPa)	Poisson's ratio ν	Convective heat transfer coefficient h (W/m^2·K)	Thermal conductivity k (W/m·K)	Coefficient of thermal expansion α (10^{-6}/K)	Specific heat c (kJ/kg·K)
370	0.22	40000	20	6.8	880

above-mentioned quenching process. A plane-stress finite element model of 20 mm × 50 mm with prefabricated cracks is used for the calculation. At first, a specimen at a uniform initial temperature T_0 is rapidly exposed to water at a temperature T_∞ on the upper surface, Fig. 2a. The size of the element can affect the accuracy of the simulation with the damage model. To obtain better calculation accuracy, the element size should be smaller than the material's characteristic length [20]:

$$l = \frac{K_{IC}^2}{2\pi\sigma_{Cr}^2} = 0.072mm \tag{1}$$

where K_{IC} = 3.84 MPa mm$^{1/2}$ and σ_{Cr} = 180 MPa are the fracture toughness and tensile strength of the ceramic [8,21]. So we choose the finite element length of 0.05 mm, with a time increment of 0.5 ms. The representative mesh is shown in Fig. 2b. For the FEM calculation of temperature field, we use the property of air to the prefabricate crack element. The thermal characteristics of the air are as follows: density ρ = 0.783 kg/m^3; specific heat c = 1.02 kJ/kg·K; thermal conductivity k = 0.037 W/m·K. To simplify the temperature calculation during quenching, it is assumed that the crack growth does not affect the thermal transfer in the specimen. The other thermal-mechanical parameters of the alumina ceramics used in the calculation are shown in Table 1 [6,8]. Since the thermal-mechanical problem is in the range of 20–300 °C, the density, Young's modulus, Poisson's ratio, and tensile strength are regarded as temperature-independent [6]. Besides, the average value of thermal conductivity, specific heat, thermal expansion coefficient and heat transfer coefficient is used in the calculations [8], as shown in Table 1. Afterward, strain and stress fields in the specimen can be calculated at any given time according to the temperature distribution and the thermoelastic theory.

3.2. Heterogeneity of the mesoscopic element

In the presented numerical model, the ceramic sheet is considered to be composed of mesoscopic elements. Due to the wide application of Weibull statistical distribution in ceramic failure, both the elastic modulus and strength of the element is assumed to follow the Weibull distribution [7]:

$$\zeta_i = \zeta_0(-\ln\omega_i)^{1/m},\ i = 1\ldots N \tag{2}$$

where ζ_0 is the initial elastic modulus or strength of ceramic, ζ_i is the elastic modulus or strength of the i-th element, ω_i is a randomly distributed number in the interval [0,1], and m is the Weibull modulus. Danzer stated that the Weibull modulus of advanced ceramics is between 10 and 20 [2], and here we choose m = 15. Tang and our previous studies also chose m = 15 [7,8].

3.3. Damage evolution of the mesoscopic element

Since most thermal-shock failures take place in the tensile mode, the tensile stress is considered only in this paper. The stress-strain relationship of the mesoscopic element is considered as follows:

$$\sigma_T(i,t) = [1 - D(i,t)]E(i,0)\varepsilon_T(i,t) \tag{3}$$

where $\sigma_T(i,t)$, $\varepsilon_T(i,t)$, $E(i,0)$, and $D(i,t)$ are the stress, strain, initial elastic modulus, and damage variable of the i-th element under the tensile mode, respectively. The damage evolution of the i-th element is considered by (Fig. 2c) [7,22]:

$$D(i,t) = \begin{cases} 0 & 0 \le \varepsilon_T(i,t) \le \varepsilon_{Cr}(i) \\ \dfrac{\varepsilon_T(i,t) - \varepsilon_{Cr}(i)\varepsilon_U(i)}{\varepsilon_U(i) - \varepsilon_{Cr}(i)\varepsilon_T(i,t)} & \varepsilon_{Cr}(i) \le \varepsilon_T(i,t) \le \varepsilon_U(i) \\ 1 & \varepsilon_T(i,t) \ge \varepsilon_U(i) \end{cases} \tag{4}$$

where $\varepsilon_{Cr}(i) = \sigma_{Cr}(i)/E(i,0)$ is the critical tensile strain of the i-th element at the elastic limit, and $\varepsilon_U(i)$ is the ultimate strain representing the complete failure of the element which is assumed to be $2\varepsilon_{Cr}(i)$ [7]. The equivalent tensile strain $\varepsilon_T(i,t)$ is considered as follows:

$$\varepsilon_T(i,t) = \sqrt{\langle\varepsilon_1(i,t)\rangle^2 + \langle\varepsilon_2(i,t)\rangle^2} \tag{5}$$

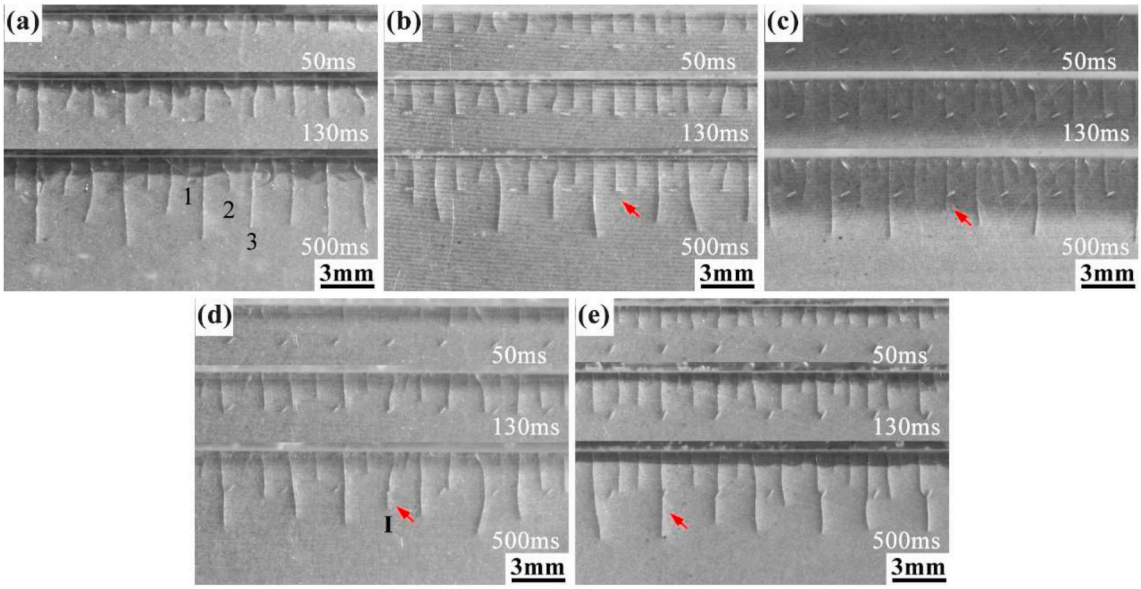

Fig. 3. Crack initiation, propagation, and interaction during quenching at a temperature difference of 300 °C with prefabricated crack angles of (a) none, (b) 0, (c) 26.6, (d) 45, and (e) 63.4°, and a crack distance of 2 mm.

Table 2
The average propagation speed of the thermal shock crack before it meets the prefabricated crack with the crack distance of 2 mm.

Prefabricated crack angles (°)	None	0	26	45	63
Crack intersected with prefabricated crack (mm/s)	15.1	14.7	15.0	15.5	15.2
Calculated value (mm/s)	15.3	15.4	14.7	15.0	14.6
Other crack (mm/s)	15.4	14.9	15.1	15.2	15.3
Calculated value (mm/s)	15.2	15.3	14.8	15.1	14.9

where $\varepsilon_1(i,t)$ and $\varepsilon_2(i,t)$ are principal strains of the i-th element, and the function <x> is expressed by

$$x = \begin{cases} x, & x \geq 0 \\ 0, & x < 0 \end{cases} \tag{6}$$

For the operation process of 3.1 and 3.2, we use the APDL language to write the command stream. It should be noted that the crack is composed of completely damaged elements.

4. Results and discussion

Fig. 3 shows the thermal-shock crack initiation, propagation, and interaction with 2 mm distance of the prefabricated crack. After the contact of the sample with water for about 500 ms, the generated cracks can be roughly divided into three levels according to the average length, i.e., 1.1, 2.2, and 4.2 mm, respectively, as shown in Fig. 3a. A similar process can be seen in the supplementary video (for clarity, the crack length in the video is 1 mm, and the playback rate is 0.3 times). The crack initiation and propagation processes in samples with various prefabricated crack angles are roughly similar; that is, the crack length hierarchy is approximate. The difference is reflected in the local region where the thermal-shock crack interacts with the prefabricated crack. In the case of specimens with 45° prefabricated crack, the second level of the thermal-shock crack I extends to the prefabricated crack at about 130 ms. After about 50 ms, secondary cracks begin to grow at the lower end of the prefabricated cracks. The angle of the secondary cracks is about 90° and the speed is similar to that of other propagating cracks, but the secondary crack will terminate when it reaches a certain extent. In other words, the length of the final crack in the vertical direction is shorter than that of other third-level cracks, i.e., about 20% shorter than the average length of the third-level crack. The kinetic energy of crack propagation after deflection seems to be insufficient, which may improve the residual strength or the toughness of ceramics [15,23].

The secondary crack length gradually becomes longer with the increment of the angle of the prefabricated crack, as marked in Fig. 3b–e. In the case of 63°, the crack length is almost the same as the third-level crack. Besides, we find that the secondary cracks appear more likely at higher angles of the prefabricated crack. Three cracks at 0° were captured by the prefabricated crack, but none at 63.4°, as illustrated in Fig. 3b–e. The average crack propagation speed before it meets the prefabricated crack is shown in Table 2, and each value is the average value of 5 cracks. Comparing the speeds of different thermal shock cracks, we can see that the crack speed is not affected when it does not interact with the prefabricated crack. It differs from the previous research of Hu or Wang that the crack growth rate will decrease when the crack interacts with the preformed defect at the nano-scale [24,25], which might be correlated with the resolution of this test that cannot assess the scale investigated in the mentioned references.

Fig. 4 depicts the simulation of the crack evolutions of samples with various prefabricated crack angles and a crack distance of 2 mm during quenching. To compare the models of cracks with different angles reliably, the random distribution of the properties of elements in the above models was the same, except for the crack elements. It can be seen that when the thermal shock cracks are not in contact with the prefabricated cracks, the thermal shock cracks of each sample, including the spacing and length hierarchy, are very close. That is, the effect of the prefabricated crack on the thermal shock crack before they are encountered is minimal. This phenomenon corresponds to the experimental results in Fig. 3. The propagation speed of the thermal-shock crack is not affected by the prefabricated crack angle when it does not intersect the prefabricated crack, Table 2. The secondary crack length gradually increases with the prefabricated crack angle, and when it reaches 63.4°, the difference between the secondary crack and the third-level crack becomes negligible, as shown in the crack A evolution, Fig. 4. Besides, we find that the secondary crack appears more likely by increasing the prefabricated crack angle. As shown in Fig. 4, there is only one crack that has the secondary cracks at 0°, but there are three at 63.4°. The above results are similar to the experiment. As shown in Fig. 4b, the original third-level crack (crack A) is prevented from propagation when it meets the prefabricated crack, and its length becomes shorter, from the length of the original third-level to the second-level. However, the adjacent

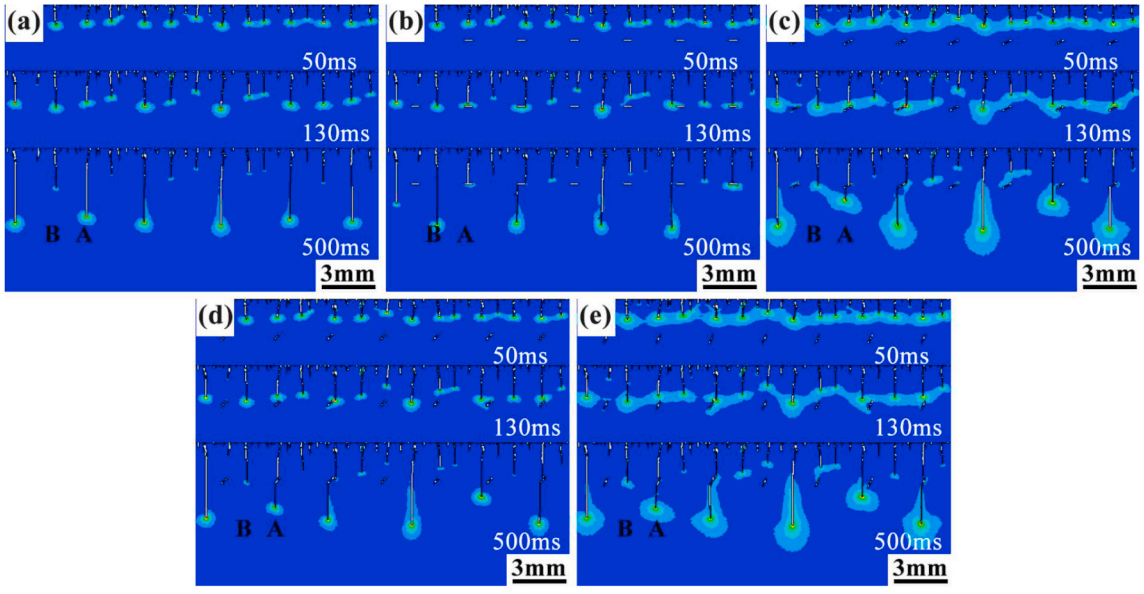

Fig. 4. Simulation of the crack evolution during quenching at a temperature difference of 300 °C with prefabricated crack angles of (a) none, (b) 0, (c) 26.6, (d) 45, and (e) 63.4°, and a crack distance of 2 mm.

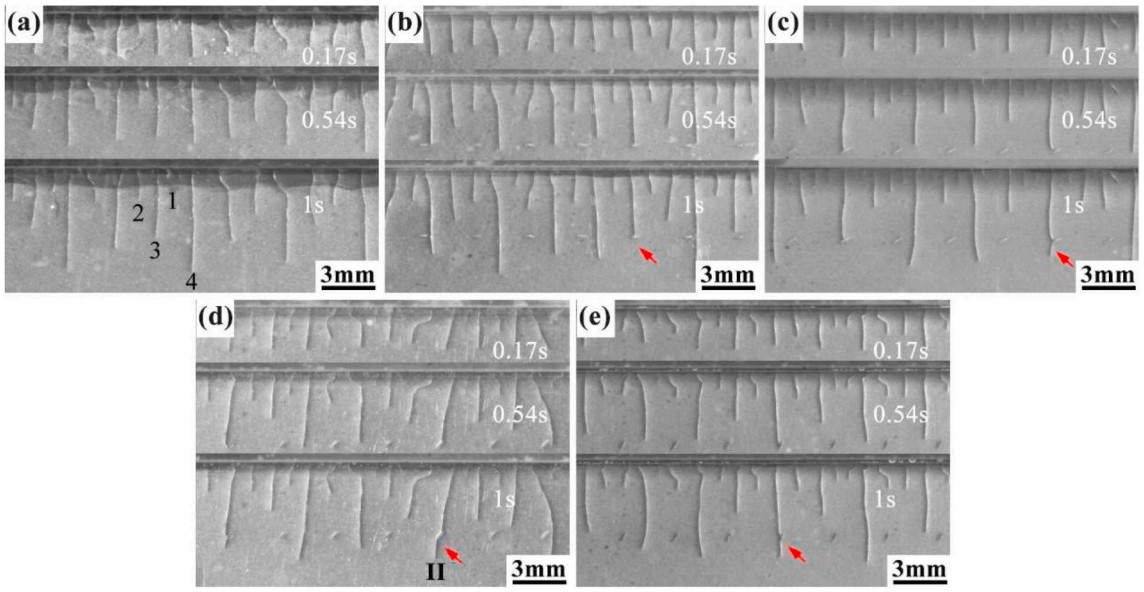

Fig. 5. Crack initiation, propagation, and interaction during quenching at a temperature difference of 300 °C with prefabricated crack angles of (a) none, (b) 0, (c) 26.6, (d) 45, and (e) 63.4°, and a crack distance of 4 mm.

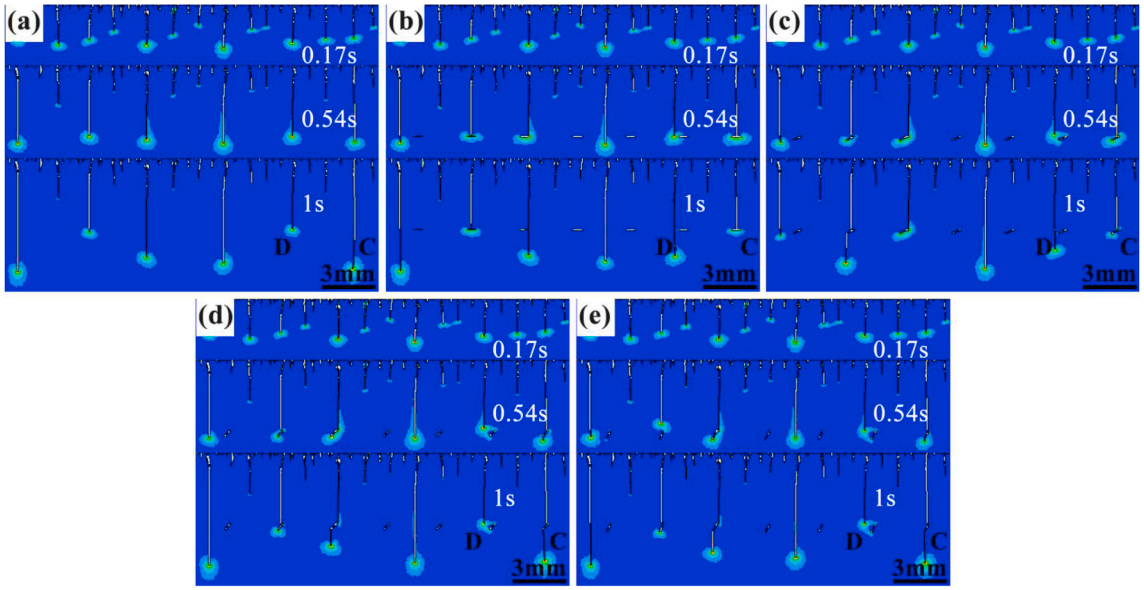

Fig. 6. Simulation of the crack evolution during quenching at a temperature difference of 300 °C with prefabricated crack angles of (a) none, (b) 0, (c) 26.6, (d) 45, and (e) 63.4°, and a crack distance of 4 mm.

original second-level crack (crack B) continues to propagate and becomes as long as the third-level crack. Thus, the existence of the prefabricated crack with a distance of 2 mm may affect the hierarchy of the second and third levels of the thermal-shock cracks. The plausible cause is that when the thermal-shock crack intersects the prefabricated crack, the thermal strain energy is rapidly released, which affects the distribution of the strain energy, so the nearby crack evolves into the third-level crack over time.

To study the influence of prefabricated crack distance on the thermal-shock cracks, we capture the crack initiation, propagation, and interaction during quenching with the prefabricated crack distance of 4 mm, Fig. 5. After 1 s of contact with water, the cracks can be roughly divided into four levels according to the length, i.e., 1.1, 2.2, 3.8, and 5.2 mm, respectively, as shown in Fig. 5a. The crack growth is similar to the case of crack distance of 2 mm. The only difference is that the third-level or fourth-level thermal-shock cracks interact with the prefabricated crack, but not the second-level crack.

The thermal-shock crack extends to the prefabricated crack at about 540 ms. After about 200 ms, a secondary crack begins to grow at the lower end of the prefabricated cracks, as shown in the evolution of crack II in Fig. 5d. The angle of the secondary cracks is about 90°. With the increment of the prefabricated crack angle, the secondary crack length gradually becomes longer, as marked in Fig. 5b–e. We find that the secondary crack appears more likely with the increase of the prefabricated crack angle; cracks are captured by the prefabricated crack at 0 and 26.6°, but none at 45 and 63.4°, Fig. 5b–e.

Fig. 6 depicts the simulation of the crack evolutions of samples with various prefabricated crack angles and crack distance of 4 mm during quenching. The crack evolution process is similar to the case of a 2 mm crack distance. The length of the secondary crack gradually increases

with the prefabricated crack angle, as shown in the evolution of crack C in Fig. 6. The probability of secondary crack occurrence increases with the angle of the prefabricated cracks: from one crack at 0 and 26.6° to two cracks at 45 and 63.4°, as shown in Fig. 6. The above results are consistent with the experimental observations. Besides, the hierarchy of crack C (fourth-level) and crack D (third-level) has changed because of the presence of prefabricated cracks, Fig. 6. Conclusively, the existence of the prefabricated crack with a distance of 4 mm may affect the hierarchy of the third level and fourth level of the thermal-shock crack. To the authors' best knowledge, there are few studies on crack propagation through preexisted cracks, and our research can provide a useful reference for crack interaction investigations.

5. Conclusions

The speed of the thermal-shock crack growth is not affected before it intersects with the prefabricated crack, as shown by the real-time thermal-shock experiments. The secondary crack may appear at the lower end of the prefabricated crack, and the total vertical length of the crack will increase with the prefabricated crack angle. The probability of secondary cracks occurrence will also increase with the angle of the prefabricated cracks. Besides, except for the different hierarchy of the cracks, the effects of the prefabricated crack distance of 2 and 4 mm on the thermal-shock crack growth are the same. We used the meso-damage mechanics model to simulate the interaction between thermal-shock cracks and prefabricated cracks, and the calculations exhibited similar results to the experiment. Therefore, the meso-damage mechanics is verified to be a suitable method for prediction of the interaction between thermal-shock cracks and a prefabricated crack.

Declaration of competing interest

The authors declare that they have no known competing financial interests or personal relationships that could have appeared to influence the work reported in this paper.

Acknowledgments

This work was sponsored by the NSFC Basic Science Center Program for "Multiscale Problems in Nonlinear Mechanics" (11988102), the Strategic Priority Research Program of the Chinese Academy of Sciences (XDB22040102 and XDC06050300), and the Natural Science Foundation of Shanghai (18ZR1417000).

Appendix A. Supplementary data

Supplementary data to this article can be found online at https://doi.org/10.1016/j.ceramint.2020.09.215.

References

[1] Y.W. Wang, B. Xia, H.H. Su, H. Chen, X. Feng, Improving the thermal shock resistance of ceramics by crack arrest blocks, Sci. China Technol. Sci. 59 (6) (2016) 913–919.
[2] R. Danzer, T. Lube, P. Supancic, R. Damani, Fracture of ceramics, Adv. Eng. Mater. 10 (2008) 275–298.
[3] A.Z. Wang, P. Hu, B. Du, C. Fang, D.Y. Zhang, X.H. Zhang, Cracking behavior of ZrB_2-SiC-Graphite sharp leading edges during thermal shock, Ceram. Int. 44 (2018) 7694–7699.
[4] W.E. Pompe, Thermal shock behavior of ceramic materials-modeling and measurement, in: G.A. Schneider, G. Petzow (Eds.), Thermal Shock and Thermal Fatigue Behavior of Advanced Ceramics, 1993.
[5] D.R. Jenkins, Optimal spacing and penetration of cracks in a shrinking slab, Phys. Rev. E 71 (5) (2005), 056117.
[6] Y.X. Liu, X.F. Wu, Q.K. Guo, C.P. Jiang, F. Song, J. Li, Experiments and numerical simulations of thermal shock crack patterns in thin circular ceramic specimens, Ceram. Int. 41 (2015) 1107–1114.
[7] S.B. Tang, H. Zhang, C.A. Tang, H.Y. Liu, Numerical model for the cracking behavior of heterogeneous brittle solids subjected to thermal shock, Int. J. Solid Struct. 80 (2016) 520–531.
[8] Y.F. Shao, B.Y. Liu, X.H. Wang, L. Li, J.C. Wei, F. Song, Crack propagation speed in ceramic during quenching, J. Eur. Ceram. Soc. 38 (2018) 2879–2885.
[9] D.Y. Chu, X. Li, Z.L. Liu, Study the dynamic crack path in brittle material under thermal shock loading by phase field modeling, Int. J. Fract. 208 (2017) 115–130.
[10] J. Li, F. Song, C.P. Jiang, Direct numerical simulations on crack formation in ceramic materials under thermal shock by using a non-local fracture model, J. Eur. Ceram. Soc. 33 (13–14) (2013) 2677–2687.
[11] Y.T. Wang, X.P. Zhou, M.M. Kou, An improved coupled thermo-mechanic bond-based peridynamic model for cracking behaviors in brittle solids subjected to thermal shocks, Eur. J. Mech. Solid. 73 (2019) 282–305.
[12] B. Bourdin, J.J. Marigo, C. Maurini, P. Sicsic, Morphogenesis and propagation of complex cracks induced by thermal shocks, Phys. Rev. Lett. 112 (2014), 014301.
[13] P. Sicsic, J.J. Marigo, C. Maurini, Initiation of a periodic array of cracks in the thermal shock problem: a gradient damage modeling, J. Mech. Phys. Solid. 63 (2) (2014) 256–284.
[14] Y.F. Shao, F. Song, B.Y. Liu, W. Li, L. Li, C.P. Jiang, Observation of ceramic cracking during quenching, J. Am. Ceram. Soc. 100 (2017) 520–523.
[15] C.K. Chen, Statistical simulation of microcrack toughening in advanced ceramics, J. Eur. Ceram. Soc. 25 (2005) 3293–3299.
[16] H. Haeri, K. Shahriar, M.F. Marji, P. Moarefvand, Cracks coalescence mechanism and cracks propagation paths in rock-like specimens containing pre-existing random cracks under compression, J. Cent. S. Univ. 21 (2014) 2404–2414.
[17] D. Misseroni, A.B. Movchan, N.V. Movchan, D. Bigoni, Experimental and analytical insights on fracture trajectories in brittle materials with voids, Int. J. Solid Struct. 63 (2015) 219–225.
[18] E. Sahouryeh, A.V. Dyskin, L.N. Germanovich, Crack growth under biaxial compression, Eng. Fract. Mech. 69 (2002) 2187–2198.
[19] M.T. Ebrahimi, D. Dini, D.S. Balint, A.P. Sutton, S. Ozbayraktar, Discrete crack dynamics: a planar model of crack propagation and crack-inclusion interactions in brittle materials, Int. J. Solid Struct. 152–153 (2018) 12–27.
[20] J. Li, D. Leguillon, Finite element implementation of the coupled criterion for numerical simulations of crack initiation and propagation in brittle or quasi-brittle materials, Theor. Appl. Fract. Mech. 93 (2018) 105–115.
[21] Y.F. Shao, R.Q. Du, X.F. Wu, F. Song, X.H. Xu, C.P. Jiang, Effect of porosity on the crack pattern and residual strength of ceramics after quenching, J. Mater. Sci. 48 (2013) 6431–6436.
[22] J. Mazars, G. Pijaudiercabot, Continuum damage theory—application to concrete, J. Eng. Mech. 115 (2) (1989) 345–365.
[23] Y.F. Shao, Y. Zhang, X.H. Xu, Z.L. Zhou, W. Li, B.Y. Liu, Effect of crack pattern on the residual strength of ceramics after quenching, J. Am. Ceram. Soc. 94 (9) (2011) 2804–2807.
[24] S. Hu, S. Wang, The influences of crystal orientation and crack interaction on the initiation of growth and propagation mode of microcrack: a phase-field-crystal study, Physica B 552 (2019) 104–109.
[25] L. Wang, Q. Liu, S. Shen, Effects of void-crack interaction and void distribution on crack propagation in single crystal silicon, Eng. Fract. Mech. 146 (2015) 56–66.